Solution Structure of the Biologically Relevant G-Quadruplex Element in the Human c-MYC Promoter. Implications for G-Quadruplex Stabilization†

Attila Ambrus,‡ Ding Chen,‡ Jixun Dai,‡ Roger A. Jones,§ and Danzhou Yang*,‡,||

College of Pharmacy, The University of Arizona, 1703 East Mabel Street, Tucson, Arizona 85721, Department of Chemistry and Chemical Biology, Rutgers University, 610 Taylor Road, Piscataway, New Jersey 08854, and Arizona Cancer Center, 1515 North Campbell Avenue, Tucson, Arizona 85724

Received August 13, 2004; Revised Manuscript Received December 17, 2004

ABSTRACT: The nuclease hypersensitivity element III_1 (NHE III_1) of the c-MYC promoter strongly controls the transcriptional activity of the c-MYC oncogene. The purine-rich strand of the NHE III_1 element has been shown to be a silencer element for c-MYC transcription upon formation of a G-quadruplex structure. We have determined the predominant G-quadruplex structure of this silencer element in potassium solution by NMR. The G-quadruplex structure adopts an intramolecular parallel-stranded quadruplex conformation with three guanine tetrads and three side loops, including two single-nucleotide side loops and one double-nucleotide side loop, that connect the four guanine strands. The three side loops are very stable and well-defined. The 3′-flanking sequence forms a stable fold-back stacking conformation capping the top end of the G-quadruplex structure. The 5′-flanking A and G bases cap the bottom end of the G-quadruplex, with the adenine stacking very well with the bottom tetrad. This paper reports the first solution structure of a G-quadruplex found to form in the promoter region of an oncogene (c-MYC). This G-quadruplex structure is extremely stable, with a similar melting temperature (>85 °C) to that of the wild-type 27-mer purine-rich NHE III_1 sequence of the c-MYC promoter. This predominant quadruplex structure has been shown to be biologically relevant, and the structural information revealed in this research provides an important basis for the design of new drug candidates that specifically target the c-MYC G-quadruplex structure and modulate gene expression.

The aberrant overexpression of the c-MYC oncogene is associated with a broad spectrum of human cancers, and its transcriptional regulation has been studied extensively (*1*−*4*). The nuclear hypersensitivity element III_1 (NHE III_1)[1] of the c-MYC promoter controls 80−90% of the c-MYC transcription level (*5*−*10*).

This NHE III_1 element can form transcriptionally active and silenced forms (*11*). The purine-rich strand of the NHE III_1 sequence is a 27-nt long, guanine-rich segment (Pu27) comprising five consecutive runs of guanines, with three runs composed of four guanines each and two runs composed of three guanines each (Figure 1). This purine-rich strand is part of the silencer element and can form a quadruplex structure that has been shown to be critical for transcriptional silencing (*12*−*14*). Mutational analysis in conjunction with a luciferase reporter system of the Pu27-mer indicates that the first run of guanines (G2−5) is not involved in the formation of the biologically relevant G-quadruplex structure, implicating the four consecutive 3′ runs of guanines as those involved in the silencer element (*12*, *15*). Specific single G-to-A mutations that destabilize the formation of the G-quadruplex structure can significantly enhance the basal transcription of c-MYC (*12*). Moreover, these same mutations are also found in 30% of human colorectal tumors along with the overexpression of the c-MYC gene (*14*). Quadruplex-interacting agents that stabilize the silencer element G-quadruplex can inhibit the c-MYC oncogene expression (*12*, *13*), indicating that this c-MYC silencer element is a good target for cancer drug development.

Several models have been proposed for the structure of the G-quadruplex present in the silencer element, mainly based upon chemical footprinting data (*7*, *12*). Very recently, a parallel-stranded quadruplex model has been proposed for the c-MYC silencer element (*15*, *16*), by using truncated sequences of this element. Oligomers containing just the four consecutive 3′ runs of guanines are the minimal prerequisite for the G-quadruplex formation and display a DMS cleavage pattern identical to that of the Pu27-mer silencer element. It has also been proposed that the Pu18-mer containing the four 3′ runs of guanines forms a mixture of four biologically relevant parallel-stranded G-quadruplexes that are in dynamic equilibrium (*15*). The proposed parallel G-quadruplex topology has been independently determined by NMR spectroscopy (*16*).

† This research was supported by the National Institutes of Health (1K01CA83886 and 1S10 RR16659).

* To whom correspondence should be addressed. Telephone: (520) 626-5969. Fax: (520) 626-6988. E-mail: yangd@pharmacy.arizona.edu.

‡ The University of Arizona.

§ Rutgers University.

|| Arizona Cancer Center.

[1] Abbreviations: NMR, nuclear magnetic resonance; NOESY, nuclear Overhauser effect spectroscopy; TOCSY, total correlation spectroscopy; DQF, double quantum filtered; COSY, correlation spectroscopy; HMQC, homonuclear multiple quantum coherence; JR, jump-and-return; HPLC, high performance liquid chromatography; AcOH, acetic acid; G, guanine; T, thymine; C, cytosine; A, adenine; Pu, purine; T_m, melting temperature; NHE, nuclear hypersensitivity element; DMT, dimethoxy-trytil; Me, methyl; VT, variable temperature; RMD, restrained molecular dynamics.

10.1021/bi048242p CCC: $30.25
Published on Web 01/14/2005

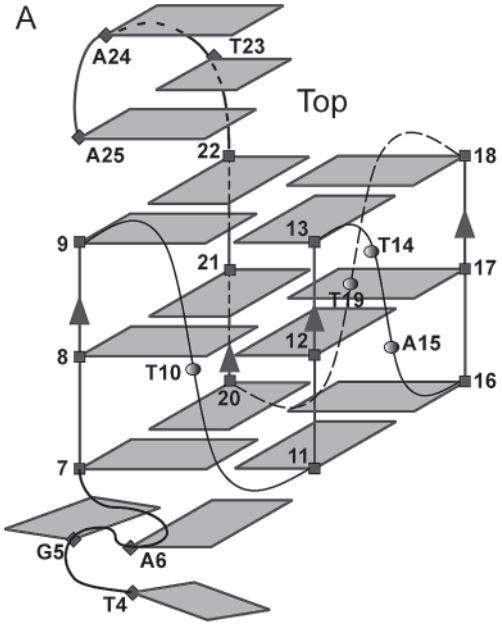

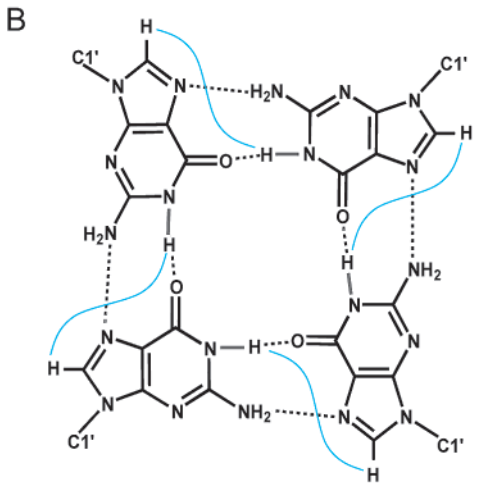

1 2 3 4 5 6 7 8 9 10 11 12 13 14 15 16 17 18 19 20 21 22 23 24 25 26 27

Pu27 TGGGGAGGGTGGGGAGGGTGGGGAAGG

Pu18 AGGGTGGGGAGGGTGGGG

MYC22 TGAGGGTGGGGAGGGTGGGGAA

MYC22-G14T/G23T TGAGGGTGGGTAGGGTGGGTAA

FIGURE 1: (A) Schematic drawing of the MYC22-G14T/G23T G-quadruplex. Guanines are represented by gray boxes. Strand directionalities are indicated by arrows. (B) H1−H8 connectivity pattern in a G-tetrad; inter-residual NOEs are detected between Hs connected by blue lines in JR−NOESY experiments. Bottom panel: The promoter sequence of the c-MYC gene and its modifications. Pu27 is the 27-mer wild-type sequence; Pu18 contains only the necessary G-runs for quadruplex formation; MYC22 is the extended Pu18 sequence that adopts one major parallel structure; MYC22-G14T/G23T represents the sequence that is investigated in this study. The numbering system is shown above Pu27.

While the c-MYC silencer element is a good anticancer drug target, a structure-based approach toward development of quadruplex-interacting agents requires atomic level information on the structure of the biologically relevant G-quadruplex. The two four-member guanine-runs in a recent NMR study (*16*) give rise to ambiguity and the possibilities of four different G-quadruplex structures for the biologically relevant sequence (Myc-2345). In this paper, we report the NMR solution structure for the predominant G-quadruplex conformer of the c-MYC silencer element (*15*). The selected sequence MYC22-G14T/G23T (Figure 1, bottom panel) contains two G-to-T mutations at residue positions 14 and 23 of the wild-type c-MYC sequence, which is predicted (*15*) to restrict the mixture of loop isomers to a single parallel-stranded G-quadruplex structure. The new structural information explains the unexpectedly high melting temperature (T_m) of the G-quadruplex and provides important new insight for structure-based design of compounds that modulate c-MYC expression.

MATERIALS AND METHODS

Sample Preparation. The DNA oligonucleotides were synthesized using β-cyanoethylphosphoramidite solid-phase chemistry on an Expedite 8909 Nucleic Acid Synthesis system (Applied Biosystem, Inc) in DMT-on mode, and were purified using C18 reverse-phase HPLC chromatography. Deprotection was carried out using 80% AcOH for 1 h, followed by ether extraction. DMT-off DNA was further purified by HPLC followed by successive dialysis against 150 mM NaCl and H_2O. 6% ^{15}N, ^{13}C-guanine phosphoramidite was used for site-specific labeled DNA synthesis. The 1,2,7-^{15}N, 2-^{13}C-labeled guanine phosphoramidite was synthesized as described in ref *17*. Samples in D_2O were prepared by repeated lyophilization and final dissolution in 99.96% D_2O. Water samples were prepared in 10%/90% D_2O/H_2O solution. The final NMR samples contained 0.2−3 mM DNA oligonucleotides in 25 mM K-phosphate, 70 mM KCl, pH 7.0.

Electromobility Shift Assay. Synthesized oligonucleotides (DMT-off) were purified by gel electrophoresis on an 8% denaturing polyacrylamide gel. The bands were excised and DNA was removed by soaking overnight in buffer. DNA was recovered by ethanol precipitation. End-labeled single-stranded oligonucleotides were obtained by incubating the oligos with terminal transferase and [α-^{32}P]ATP for 1 h at 37 °C. Labeled DNA was purified with a Bio-Spin 6 chromatography column (BioRad) after inactivation of the kinase by heating at 70 °C for 8 min. The labeled oligonucleotides were purified again by gel electrophoresis on a 12% denaturing gel. The bands were excised and the DNA was removed by soaking in water overnight while shaking. Purified labeled oligonucleotides were diluted to 2 μM, heated to 95 °C, and slowly cooled to room temperature in a buffer (100 mM Tris-HCl/1 mM EDTA, pH 7.5, 100 mM KCl). After annealing, oligonucleotides were subjected to native preparative gel electrophoresis (15% polyacrylamide, 100 mM KCl, 20 h, 4 °C). The dried gels were quantified on a Molecular Dynamics Phosphorimager system (Amersham Biosciences).

NMR Experiments. NMR experiments were performed on a Bruker DRX-600 spectrometer. Identifications of guanine imino and H8 protons in site-specific labeled oligonucleotides were performed by a one-dimensional gradient HMQC experiment that used presaturation for water suppression (will be reported elsewhere). Standard homonuclear 2D NMR experiments, including DQF−COSY, TOCSY, and NOESY, were used to assign the nonexchangeable proton chemical shifts. The NMR experiments for samples in water solution were performed with presaturation or jump-and-return water suppression techniques. Relaxation delays were set to 3 s.

The acquisition data points were set to 4096 × 512. The 60-degree shifted sine-squared functions were applied to both dimensions of NOESY and TOCSY spectra. The five-order polynomial functions were employed for the baseline corrections. The final data points were 4096 × 1024. Peak assignments and integrations were achieved using the software Sparky (UCSF). Distances between nonexchangeable protons were estimated based on the NOE cross-peak volumes at 50−250 ms mixing times, with the upper and lower boundaries assigned to ±20% of the estimated distances. The sugar methylene proton H2′−H2″ distance of T23 (1.76 Å, isolated NOE cross-peak) was used as a reference. Distances between exchangeable protons were assigned to weak, medium, or strong groups with looser boundaries (±1 Å). Unresolved protons were replaced by pseudo-atoms, and the appropriate correction was applied to the measured distance.

NOE-Distance Restrained Molecular Dynamics Calculations. Structure calculations were performed using NOE-restrained molecular dynamics simulation in the software package Insight II/Discover III (version 2000.1, Accelrys, CA). The molecular model from a recent study by Seenisamy et al. (*15*) was kindly provided by Dr. Laurence Hurley and was used as the start point. The 5′-flanking TGA and 3′-flanking TAA sequences were added to the structure, with the conformations deduced from the NOE data (see Results and Discussion). The conformations of the three double-chain-reversal side loops were also modified according to the NOE data. Two K^+ ions were included between the G-tetrad planes to stabilize the tetrad structure. Potassium ions were used to counter the negative charge of DNA backbone. This starting model of MYC22-G14T/G23T was then soaked into water solvent using 10 Å water layer in Insight II. A CFF force field in Insight II is suitable for DNA and was used for all the calculations (*18*). The cell multipole nonbond method was used in the calculation. The complete molecular system was first subjected to energy minimization to the system convergence of 1 kcal mol^{-1} $Å^{-1}$. The energy-minimized molecular system was then subjected to a distance-restrained molecular dynamic (RMD) simulation at 300 K. The flat-bottom energy function was used for distance constraints from NOE data, with the force constants of 100 kcal mol^{-1} $Å^{-2}$. A total of 246 NOE distance restraints, of which 61 are from interresidue NOE interactions, were incorporated into the restrained molecular dynamics calculation. Hydrogen bond restraints were applied to the G-tetrads, using a quadratic energy function with a force constant of 200 kcal mol^{-1} $Å^{-2}$. Molecular dynamics was first equilibrated for 20 ps with time steps of 1 fs and continued for 80 ps simulations. Dynamic trajectories were recoded every 0.5 ps for analysis. Individual simulations from the point of a stable trajectory generated time-averaged structures. The 20 lowest energy structures were extracted from the MD simulations, which were energy minimized to 1 kcal mol^{-1} $Å^{-1}$. The average rms deviation is 0.88 Å for the family of 20 structures.

Molecular Computer Modeling of MYC22-G14T. The lowest energy structure of the MYC22-G14T/G23T from the NOE-restrained molecular dynamics refinement was modified by replacing the T23 with the wild-type G23. The modified structure was soaked in water solvent and subjected to energy minimization to a gradient of less than 1 kcal mol^{-1} $Å^{-1}$. The energy-minimized structure was then subjected to a molecular dynamics calculation with 20 ps equilibration and 80 ps simulations at 300 K, while only the G22-A25 were allowed to move. Dynamics time step was 1 fs and dynamic trajectories were recoded every 0.5 ps for analysis. The lowest energy structure from the dynamics simulation was subjected to further energy minimization to a convergence of 1 kcal mol^{-1} $Å^{-1}$.

Molecular modeling calculations were performed using Insight II/Discover III software package (version 2000.1 Accelrys, CA). The CFF force field was used for all of the calculations, with the nonbond cell multipole method. The energy minimization was carried out by using the conjugate gradient method until the system convergence was reached.

RESULTS AND DISCUSSION

Modified c-MYC 22-mer (MYC22-G14T/G23T) with Two G-to-T Mutations Forms a Single G-Quadruplex Structure in K^+ Solution. The four consecutive 3′-runs of guanines in the human c-MYC silencer element forms a mixture of four G-quadruplex isomers (*15*). The wild-type c-MYC sequences Pu27-mer and Pu18-mer (the minimal sequence for G-quadruplex formation) (Figure 1) display broad envelopes in one-dimensional ^1H NMR (data not shown), indicating a dynamic equilibrium of multiple conformers. Appropriate double G-to-T mutations can single out the four isomers one by one (*15*), while the isomer with dual mutations at positions 14 and 23 is shown to be the predominant conformation in the mixture. Proper extensions of the Pu18 can also stabilize the G-quadruplex structure (*16*), and therefore this insight was used in combination with the G-to-T dual mutations for design of our oligomer for NMR structure determination. The 1D NMR spectrum of this 14,23-G-to-T mutant c-MYC sequence (MYC22-G14T/G23T, Figure 1) in potassium solution shows improved line width and better resolution (upper, Figure 2A) compared to that of the wild-type sequence (lower, Figure 2A). The NMR samples were all prepared in 70 mM KCl and 25 mM potassium phosphate at pH 7.0. Potassium cation has been shown to be required for the formation of the biologically relevant G-quadruplex structure in the purine-rich c-MYC silence element (*12*). We used a total of 95 mM K^+ concentration because it is close to the physiological K^+ concentration and it provides the stability of this G-quadruplex.

The sharp NMR spectral line widths (Figure 2A) implicate the presence of an intramolecular monomeric structure. The presence of a single unimolecular structure was confirmed by an EMSA experiment (Figure 3). The stoichiometry determined by NMR titration experiment (*16*) is also consistent with a monomeric structure (data not shown).

Proton Resonance Assignment of MYC22-G14T/G23T. The imino proton resonances located between 10.5 and 12 ppm indicate the formation of a G-quadruplex structure (*19*−*24*). The presence of 12 imino peaks is consistent with the existence of three G-tetrads. The guanine imino and base H8 protons of MYC22-G14T/G23T were unambiguously assigned by the site-specific incorporation of 1,2,7-^{15}N, 2-^{13}C-labeled guanine nucleoside at each guanine position of the sequence. The guanine imino proton resonances (one bond coupling to N1) and the base H8 proton resonances (two bond coupling to N7) were identified by one-dimensional

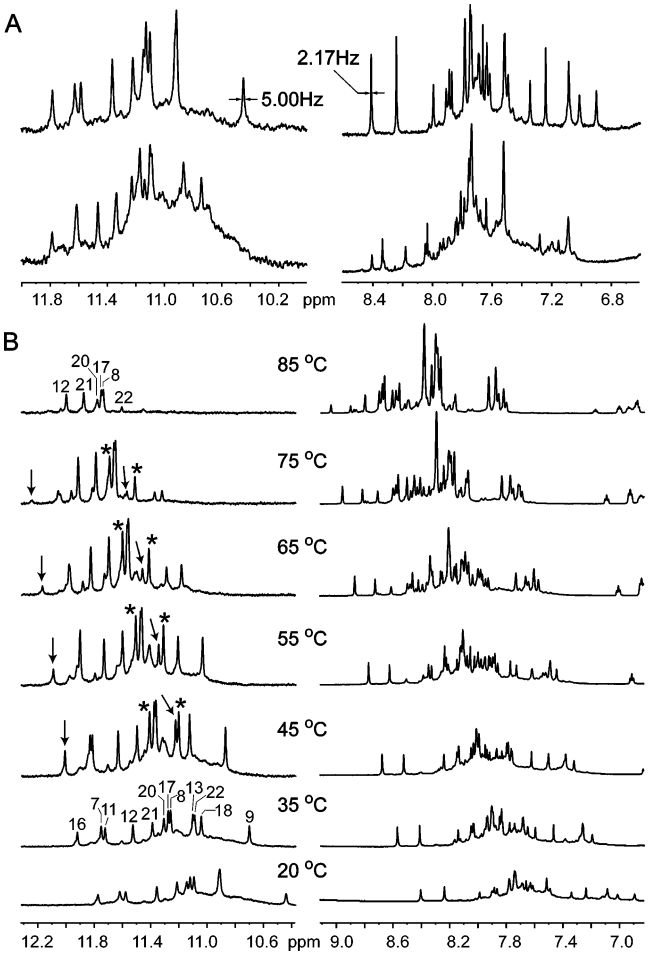

FIGURE 2: (A) One-dimensional proton NMR spectra of MYC22-G14T/G23T (upper) and MYC22 (lower) (see Figure 1 for sequences), imino and aromatic regions. The mutated sequence shows better resolution and narrower line widths compared to the wild-type one. Experimental conditions: 20 °C, 25 mM K-phosphate, 70 mM KCl, pH 7.0, 0.2 mM DNA. (B) Imino and aromatic proton regions in a VT study of MYC22-G14T/G23T. All imino protons of tetrad guanines are labeled at 35 °C. Imino protons of G20 and G22 are further labeled with asterisks, and imino protons of G16 and G13 are labeled with arrows. Conditions: 25 mM K-phosphate, 70 mM KCl, pH 7.0, 1 mM DNA. All spectra are plotted on an absolute scale.

presaturation HMQC experiments [Figure S1 (Supporting Information) and 2B].

The base H6 proton resonances of thymines were unambiguously assigned by substituting deoxyuridine (dU) for dT at each thymine position in the MYC22-G14T/G23T sequence. Complete assignment of nonexchangeable base and sugar proton resonances of MYC22-G14T/G23T was accomplished by using 2D-NOESY, TOCSY, and COSY data at 25 °C. The chemical shifts of all resonances are listed in Table 1.

G-Tetrad Alignments of the MYC22-G14T/G23T G-Quadruplex Structure. G-tetrad alignments are determined by the interresidue connectivities of H8 and H1 protons in exchangeable proton NOESY spectra. In a G-tetrad plane, the base H8 of one guanine is in close spatial vicinity to the imino H1 of the adjacent guanine due to the Hoogsteen H-bond network of the G-tetrad (Figure 1B), and their NOE connectivities can be detected. The through-space H8/H1 connectivities define the topology of a tetrad plane. For example, the G7H1/G11H8, G11H1/G16H8, G16H1/G20H8, and G20H1/G7H8 NOE interactions (Figure 4A) define a tetrad plane of G7-G11-G16-G20 (Figure 1A,B). Two other tetrad planes, G8-G12-G17-G21 and G9-G13-G18-G22, can also be determined in this way (Figure 1A). The glycosidic torsion angles of all guanines are in the anti conformation as indicated by the intraresidue H8−H1′ NOE intensities (Figure 4B). From these data, the alignment of the MYC22-G14T/G23T G-tetrads is defined (Figure 1A). In accord with the wild-type topology (*15*, *16*), MYC22-G14T/G23T adopts a parallel-stranded G-quadruplex with 1:2:1 side loops of T, TA, and T, respectively. The intramolecular parallel-

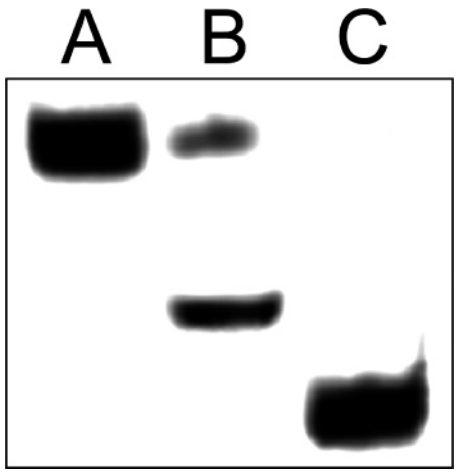

FIGURE 3: Electrophoretic gel mobility shift assays of a random 22-mer DNA oligonucleotide (5′-AGATGATGAAGTAGGTA-GAAAT) (A), an intermolecular dimer G-quadruplex (2 × DNA 22-mer 5′-GGGGTTTGGGGGGGGTTTGGGG) (B), and the MYC22-G14T/G23T DNA (C). The intramolecular G-quadruplex formed in MYC22-G14T/G23T moves the fastest (C), while the intermolecular G-quadruplex dimer moves slower (lower band in B), and the random 22-mer DNA oligonucleotide, which is most likely to be single-stranded DNA, moves the slowest (A, and upper band in B). This result confirms the formation of a single, unimolecular structure in the MYC22-G14T/G23T sequence.

Table 1: ^{1}H NMR Chemical Shifts of MYC22-G14T/G23T at 25 °C[a]

	H6/H8	H2/Me H1/H3	H1′	H2′,H2″	H3′	H4′	H5′,H5″
T4	7.214	1.656	5.787	1.621/2.053	4.431	3.814	3.467
G5	8.010		5.905	2.426/2.602	4.860	4.060	3.691/3.870
A6	7.642	7.789	5.680	2.503/2.417	4.731	4.114	3.741/3.817
G7	8.024	11.741	6.066	2.767/3.020	5.006	4.465	4.065/4.142
G8	7.726	11.221	6.132	2.628/2.909	5.031	4.543	4.287
G9	7.751	10.605	6.417	2.779/2.599	5.139	4.613	4.291/4.359
T10	7.833	1.978	6.515	2.476/2.713	5.074	4.569	4.258/4.339
G11	7.989	11.699	6.146	2.470/2.921	5.121	4.471	4.280/4.341
G12	7.906	11.488	6.147	2.668/2.870	5.077	4.476	4.190/4.261
G13	7.867	11.053	6.434	2.771/2.603	5.042	4.487	4.280
T14	7.643	1.933	6.233	2.213/2.450	4.706	3.858	3.711
A15	8.531	8.370	6.688	3.091/2.973	5.191	4.592	4.208/4.311
G16	8.109	11.898	6.171	2.638/2.966	5.026	4.470	4.158/4.264
G17	7.803	11.247	6.197	2.688/2.968	5.025	4.554	4.215/4.303
G18	7.807	11.029	6.461	2.733/2.624	5.139	4.629	4.305/4.397
T19	7.869	1.989	6.534	2.474/2.679	5.117	4.616	4.293/4.343
G20	7.901	11.273	5.991	2.347/2.802	5.101	4.453	4.263/4.330
G21	7.898	11.345	6.039	2.674/2.741	5.077	4.524	4.191/4.256
G22	7.614	11.048	6.174	2.549/2.827	4.989	4.527	4.232/4.305
T23	7.151	1.490	5.917	1.925/2.409	4.794	4.200	4.104/4.185
A24	7.762	7.080	5.752	1.989/2.475	4.584	4.276	3.736/4.045
A25	7.486	7.378	5.605	2.195/2.376	4.438	3.938	3.463/3.767

[a] The chemical shifts are measured in 25 mM K-phosphate, 70 mM KCl, pH 7.0 referenced to DSS.

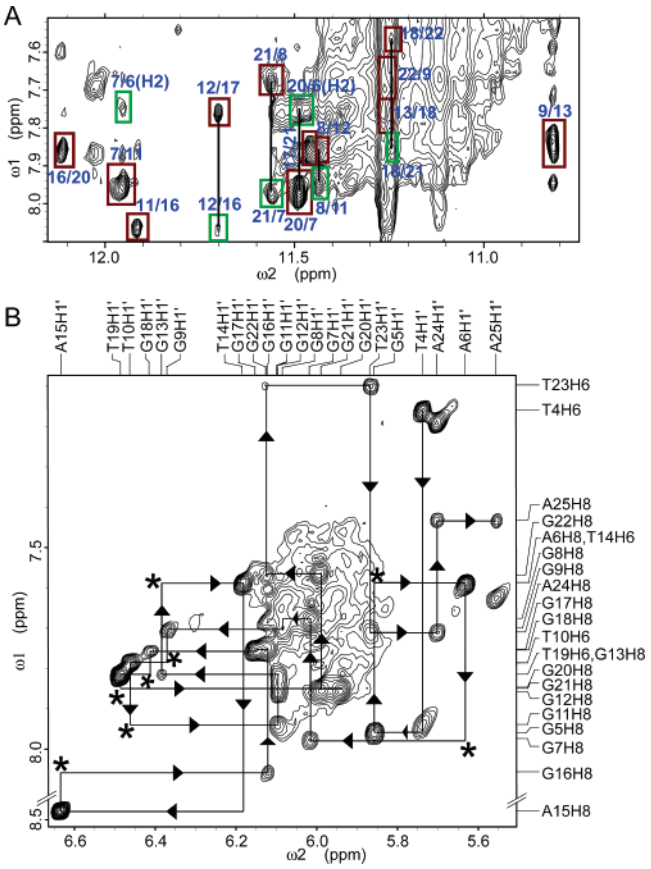

FIGURE 4: (A) The expanded H1−H8 region of the exchangeable 2D JR−NOESY spectrum of MYC22-G14T/G23T. Cross-peaks are labeled using the [(H1) guanine residue number/(H8/H2) guanine residue number] pairing system. The H2 protons are specified within parentheses. The interresidue connectivities within a tetrad plane are designated with red boxes. Green boxes label additional cross-peaks. Solid straight lines represent intertetrad connectivities. (B) The expanded H8(H6)-H1′ region of the nonexchangeable 2D-NOESY spectrum. The sequential assignment pathway is shown. Missing connectivities are labeled with asterisks. Conditions: 25 °C, 200 ms mixing time; 25 mM K-phosphate, 70 mM KCl, pH 7.0, 2 mM DNA.

stranded G-quadruplexes have been reported before on several other sequences (*20*, *25*, *26*).

MYC22-G14T/G23T G-Quadruplex Structure Is Very Stable. 1D proton spectra of MYC22-G14T/G23T at various temperatures (VT) indicate that this quadruplex structure is extremely stable (Figure 2B). The melting temperature ofMYC22-G14T/G23T in 95 mM K^+ is over 85 °C and cannot be measured by the NMR technique. This melting temperature is significantly higher than that of the Pu18-mer G14T/G23T dual mutant (68−72 °C) (*15*). Even at 85 °C, the imino resonances of G8, G12, G17, G21, G20, and G22 (weaker) are still clearly observable, indicating that the stable G-tetrads still exist, which is also supported by the base H8 proton resonances. G8, G12, G17, and G21 are the four guanines of the central tetrad (Figure 1A), consistent with the aforementioned imino assignments. Interestingly, G20 and G22 imino protons are also quite stable in the VT study, which are related to the capping effects of the terminal flanking sequences (see below).

The stability of the MYC22-G14T/G23T G-quadruplex is further supported by the H_2O-D_2O exchange experiments. As shown in Figure S2 (Supporting Information), the imino proton resonances of the four guanines (G8, G12, G17, and G21) from the central tetrad are extremely stable against exchange from H_2O to D_2O and therefore are not solvent accessible. These four imino protons are still observable even after one week of storage at 4 °C. Consistent with the VT study, the exchange of the G22 imino resonances is significantly slower than that of the rest of the guanine imino protons (data not shown).

The G12 imino proton does not display any sign of the lability and fast exchange that was observed in the wild-type sequence without G-to-T mutations (*16*), suggesting that the G14-to-T14 mutation eliminates the involvement of the G14 residue in the dynamic interconversion process of multiple isomers (*15*).

NOE connectivities of the G-tetrad guanines show that the three G-tetrads are connected by four parallel right-handed guanine strands.

Figure 4B shows an expanded NOESY spectrum of base and sugar H1′ protons. The sequential NOE cross-peak connectivities of the base H8 protons to the 5′-flanking residue sugar H1′/H2′/H2″ protons, typical for right-handed DNA twist, are also observed for the four consecutive guanine sequences (G7-G9; G11-G13; G16-G18; G20-G22) of MYC22-G14T/G23T. The sugar backbones of the guanine strands of MYC22-G14T/G23T G-quadruplex are more compact than regular B-DNA, as evident from the NOE cross-peaks between the sugar H1′ and its 3′-flanking sugar H4′ or H5′,″, e.g., G7H1′/G8H5′,″; G8H1′/G9H5′,″; G17H1′/G18H4′,H5′,″; G20H1′/G21H5′,″; G21H1′/G22H5′,″. The guanines on each of the four strands connecting three tetrads are very well stacked, as indicated by the clear NOE connections of adjacent guanine H8 protons, such as G7H8/G8H8, G11H8/G12H8, G16H8/G17H8, and G21H8/G22H8 (Figure 5).

Similar patterns of chemical shifts are observed for the guanines from the same tetrad (such as G7/G11/G16/G20 and G9/G13/G18/G22), indicating a relatively similar conformation of the four guanine strands connecting the three G-tetrads. The H2′ protons of G9, G13, and G18 are more downfield relative to the H2″ protons, characteristic of the terminal sugars whose H2′/H2″ are exposed to solvent. These are guanines from the top G-tetrad and are involved in the DNA double-chain-reversal.

Intertetrad NOE interactions are also observable in the exchangeable proton NOESY spectra, including G8H1/G11H8, G18H1/G21H8, G21H1/G7H8, and G12H1/G16H8 (Figure 4A), which span through the four side grooves of the G-tetrads (Figure 1A). These NOE interactions are consistent with a right-handed DNA backbone structure of the G-quadruplex. Among these NOE interactions, the G12H1/G16H8 connects through the double nucleotide loop (T14A15) and is weaker than other NOE interactions.

NOE Interactions of the Three Side Loops Show that They Are Double-Chain-Reversal Loops and Are Mostly Exposed to Solvent. NOE connectivities are interrupted at G9-T10-G11, G13-T14-A15-G16, and G18-T19-G20 steps (which are labeled by an asterisk in Figure 4B), consistent with the fact that T10, T14-A15, and T19 are located in the double-chain-reversal side loops (Figure 1A). Two thymines in the single nucleotide loops (T10 and T19) are in the anti conformations as indicated by the medium H6−H1′ NOE intensities in 50 ms NOESY (data not shown). The chemical shifts of all resonances from these two thymines are very

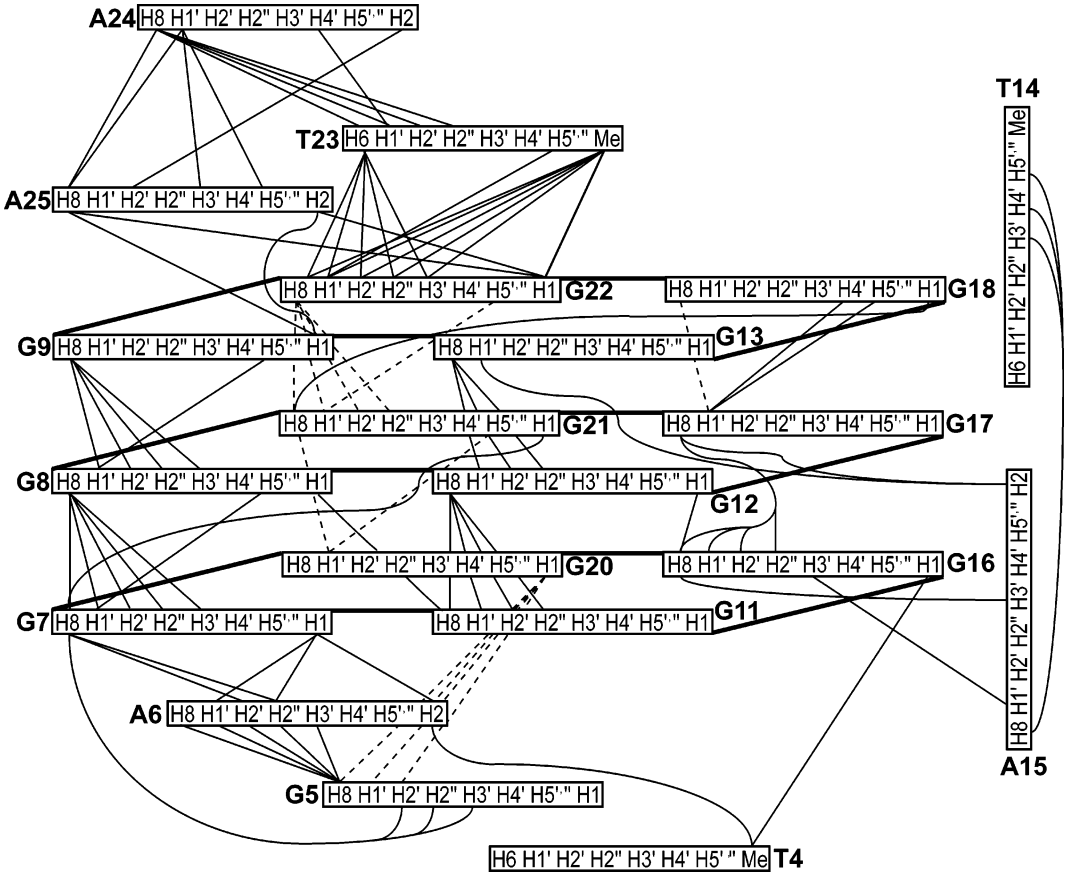

FIGURE 5: Schematic diagram of interresidue NOE connectivities of the MYC22-G14T/G23T G-quadruplex. Connectivities of the 3′-(T23-A24-A25) and 5′-(T4-G5-A6) extensions and one double-nucleotide side loop (T14A15) are shown by both solid lines and dashed lines. The NOE connectivities clearly define the quadruplex conformation and provide distance restraints for structure calculation.

close, suggesting a similar conformation and environment of the two single T side loops. The H6, methyl, and H1′ protons of T10 and T19 are downfield shifted, implying that they are well exposed to solvent.

The thymine T14 in the double nucleotide side loop (T14A15) is also in the anti conformation and is exposed to solvent. The H2 end of the A15 base points toward the G-quadruplex groove, as indicated by the weak NOE interactions of A15H2 with G13H1′ and G17H8 (Figure 5). The relatively strong NOE cross-peaks between A15H8 and T14H3′, H4′, and H5′,″ suggest that the H8 end of the A15 base points toward the T14 sugar. The H8 and H1′ resonances of A15 are markedly downfield shifted, in accord with the solvent exposure of this loop residue.

The two single nucleotide loops and the one double nucleotide loop conformation are very stable, as there is no sign of multiple conformations for either side loop. The line widths of resonances from the T19 and T14A15 side loops are in the same range as those of other tetrad guanines, whereas the line widths of T10 are broader, suggesting that T10 is involved in more internal motion on the NMR time scale.

NOE Interactions of the 3′-Flanking TAA Sequence Show that It Forms a Stable Fold-Back Conformation Stacking with the top G-Tetrad. Interresidue NOE connectivities are clearly observable within the 3′-flanking TAA sequence. T23 is very well stacked with G22, as is evident by the clear NOE interactions of T23H6/G22H8, T23H6/G22H1′ (Figure 4B), T23H6/G22H2′,H2″ and T23Me/G22H1 (Figure 5). The sequential connectivities of T23-A24-A25 are clearly observable, including A24H8/T23H1′,H2′,H2″; A25H8/A24H1′,-H2″ (Figures 4B and 5). The NOE interactions between adjacent base protons are also clearly observable, including T23H6/A24H8 and A24H8/A25H8, implying a continuous stacked conformation of the 3′-flanking TAA sequence. Multiple interresidue NOE connectivities of the sugar backbone are also observed for this three-residue flanking sequence (Figure 5).

Interestingly, NOE interactions are clearly observed between A25H8/G9H1, A25H2/G9H1, A25H8/G22H1, and A25H2/G22H1 (weaker) (Figure 4A), indicating that the 3′-terminal residue A25 is stacking over the top G-tetrad, specifically, with G22 and G9. Taking all these data into account, the stacking orientations of the 3′-flanking sequence can be defined. T23 and A25 are stacked over the top G-tetrad, while T23 is connected and stacked with G22 and the A25 residue is stacked with the G9 residue (Figure 1A). In accord with this stacking conformation, all resonances of A25 and T23 are significantly shifted to a more upfield region induced likely by the ring-current effects of the stacking guanines from the top tetrad. In addition, the H1 resonance of G9 is markedly upfield shifted, due to the same ring current effect of the stacking A25 residue. Furthermore, as previously mentioned, the imino proton H1 of G22 is significantly more stable than the imino protons of other top-tetrad guanines, which indicates that the stacking T23 and A25 are likely to form a stable H-bonded conformation above

G22 so that the G22 imino proton is protected from solvent access.

Clear connectivities observed between T23 and A24 (Figure 4B) indicate that the A24 base is stacked with the T23 residue. The H2 proton of A24 is markedly upfield shifted and displays relatively strong NOE interactions with the A25 sugar protons H2′,″(Figure 5), suggesting that the H2 end of the A24 base is stacked on the A25 residue.

NOE Interactions of the 5′-Flanking TGA Sequence Show that the A and G Residues Cover the Bottom End of the G-Quadruplex, with the Adenine Stacking with the Bottom G-Tetrad. The interresidue connectivities of the 5′-flanking TGA sequence are less straightforward compared to the 3′-flanking sequence. Several interresidue NOEs are observed between G5, A6, and G7 residues; however, the connectivities are different from those of the regular right-handed DNA structures. The NOE connectivities of a regular right-handed DNA are much weaker at the A6-G7 step, including G7H8/A6H1′ (missing) and G7H8/A6H2′,″ (weak). No NOE interaction exists for A6H8 and G5 sugar protons H1′, H2′, H2″; however, G5H8 has several weak NOE cross-peaks with A6 sugar protons (e.g., G5H8/A6H1′, H2″, Figure 5), indicating that the sugar backbone at the G5-A6 step does not adopt the regular right-handed twist DNA conformation. The regular sequential connectivities at the T4-G5 step are very weak, as indicated by the absence of NOE cross-peaks between G5 and T4 protons.

Several NOE interactions are observed between this 5′-overhanging sequence and the bottom G-tetrad. First, A6H2 has clear NOE interactions with the imino protons of G20 and G7 (Figure 4A). In addition, the imino proton of the flanking G7 shows NOE interactions with A6H1′ and H2″ (Figure 5). These NOE interactions indicate that the A6 base is stacking to the bottom G-tetrad, specifically, with G7 and G20. On the other hand, the imino proton of G20 has several observable NOE interactions with G5 protons, including G20H1/G5H8, G20H1/G5H1′, and G20H1/G5H2′. Moreover, there are several weak NOE cross-peaks between G7H8 and G5H2′, H2″ and H3′. These data suggest that the G5 residue is located close to the G20 and G7 bases as well. Only a few weak NOE cross-peaks are detectable for the T4 residue, including T4Me/A6H2 and G16H1. The lack of most NOE cross-peaks between T4 protons and other residues indicate that T4 is likely to position below the G5 and A6 residues and is more extended to solvent.

Interestingly, the imino proton H1 of G20 is significantly more stable than the imino protons of other bottom-tetrad guanines in the VT study; however, this phenomenon is not as obvious in the H_2O-D_2O exchange experiments. In addition, the chemical shift of G20H1 is not upfield shifted, as observed for the G9H1 from the top tetrad. These data suggest that, while the bottom tetrad formation is much stabilized by A6 and G5, the G20 imino proton is not as much protected from solvent access, as in the case of G22 of the top tetrad. Furthermore, even though the A6 base is well stacked, the G5 residue does not seem to stack well with the bottom tetrad.

Multiple Conformations of the Flanking Sequences. More than one chemical shift is observed for the methyl protons of T23 and T4 in the NOESY spectra at 25 °C. This phenomenon becomes much more apparent at 10 °C (Figure S3, Supporting Information). For the 3′-flanking TAA sequence, one additional set of resonances is observable for G22, T23, A24, and A25, while their sequential connectivity pathways can be traced (Figure S3, Supporting Information). This minor conformation appears to be stable and not exchanging with the major conformation on the NMR time scale, since no exchange NOE cross-peaks were observed. This minor set of resonances of the 3′-TAA overhanging sequence becomes very weak, yet still observable, at 25 °C.

Additional resonance is clearly observed for T4 in the 5′-flanking TGA sequence (Figure S3, Supporting Information); this resonance is also observable at 25 °C, indicating that the terminal T4 can adopt multiple stable conformations. No exchange cross-peaks were observed for T4 either. The phenomenon of slow exchanging resonances, such as imino protons, has also been observed in a number of previous studies of G-quadruplexes (*24*, *27*−*30*).

NOE-Restrained Structure Calculation. The NMR data define a parallel G-quadruplex as shown in Figure 1A. The starting model of MYC22-G14T/G23T was constructed based on the molecular model from a recent paper of Seenisamy et al. (*15*), which was kindly provided by Dr. Laurence Hurley, with additional 5′- and 3′-external flanking sequences and modified side loops (see Materials and Methods). Two K^+ ions were positioned between the G-tetrad planes to stabilize the tetrad structure. Potassium counterions and water solvent are included for calculation. Many interresidue NOE cross-peaks are observed in 2D-NOESY and are summarized in Figure 5. This starting molecular system was subjected to NOE-restrained molecular dynamics (RMD) calculation in Insight II/Discover III (version 2000.1, Accelrys, CA). A total of 246 distance restraints, of which 61 are from interresidue NOE interactions, were incorporated into the RMD calculation. The RMD calculation produced a family of refined structures, with the average rmsd being 0.88 Å, including all atoms for the 20 lowest energy structures. The superimposition of the 10 lowest energy structures is shown in Figure 6 (PDB ID 1XAV). The average rmsd value for each residue from the 20 lowest energy structures, including hydrogen atoms, is plotted in Figure 7. The rmsd values of G7, G11, and G16, which are the 5′-guanines of three G-strands, are larger than those of the rest of the residues, indicating a larger structural deviation of these three guanines.

Structure of MYC22-G14T/G23T G-Quadruplex. A representative model of the MYC22-G14T/G23T G-quadruplex structure is shown in two different views in Figure 8A,B. The G-quadruplex consists of three G-tetrads with four parallel DNA strands that are linked by three double-reversal side loops, in accord with previous results (*15*, *16*). Both T10 and T19 adopt a single nucleotide loop conformation connecting two parallel G-strands. Both of the single nucleotide loops adopt very similar conformations, with an extended sugar backbone strand, while the thymine base sticks out to the solvent (Figure 9A,B). This is the first example of a parallel G-quadruplex with single-nucleotide, double-chain reversal loops, which appear to be very stable. As shown in the structure, the right-handed twist of the two adjacent DNA strands makes the 3′-end of one G-strand (e.g., G9) very close in space to the 5′-end of the next G-strand (e.g., G11) so that the single nucleotide loop conformation is quite favored. The sugar backbone of the double nucleotide T14A15 loop (Figure 9B) is not as extended as the single

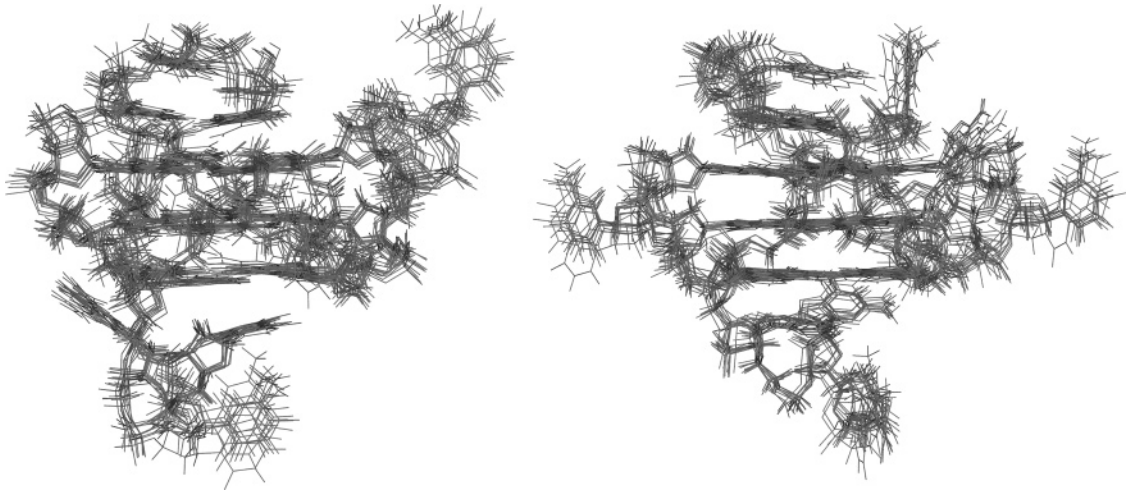

FIGURE 6: Superimposed 10 lowest energy structures of the MYC22-G14T/G23T G-quadruplex by NOE-restrained molecular dynamics calculation. Two views with a 90° rotation are shown.

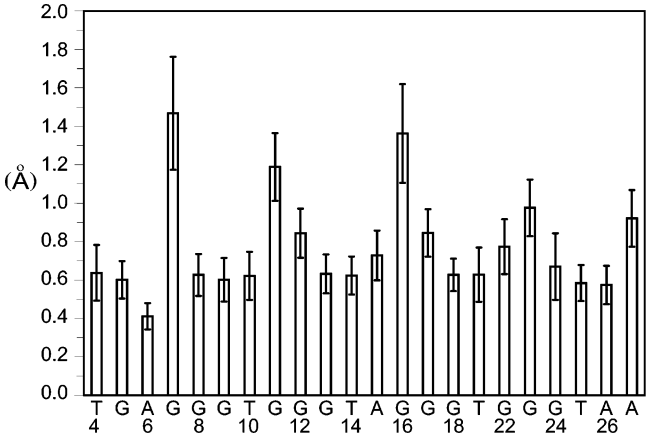

FIGURE 7: RMSD value per residue after superimposition with respect to the average coordinates of the 20 lowest energy refined structures of the MYC22-G14T/G23T G-quadruplex for all atoms. Bars represent the average RMSD value and the error bars show the standard deviation.

thymine loops, while the thymine T14 base sticks out to the solvent and the adenine A15 base is located toward the G-tetrad groove with the H2 end pointing to the top of the quadruplex. This 1:2:1 loop arrangement results in a very stable parallel G-quadruplex conformation, as demonstrated by the significant stability of the structure (T_m > 85 °C).

The four parallel G-quadruplex strands adopt similar conformations. The line widths of H8 protons of the central tetrad guanines G8 and G21 in two G-strands not connected by a side loop are relatively broader than those of other tetrad guanines, suggesting that those bases are undergoing some degree of internal motion. The widths of the four tetrad grooves are similar.

The single nucleotide T-loop may be more stable compared to the double nucleotide TA-loop. In the variable temperature study, the two most unstable, and therefore the first to disappear, guanine imino protons are those of G16 and G13 (Figure 2B). These are the guanines connecting the double nucleotide TA-side loop, indicating that the two ends of the TA-loop are the first melting points of the MYC22-G14T/G23T G-quadruplex structure.

The 3′-flanking TAA adopts a well-defined fold-back structure, capping the top end of the MYC22-G14T/G23T G-quadruplex structure (Figure 10A). The terminal A25 folds back to stack with G9 of the top G-tetrads, whereas the T23 base stacks on top of the G22 residue. The 3′-TAA overhanging sequence still somewhat follows the right-

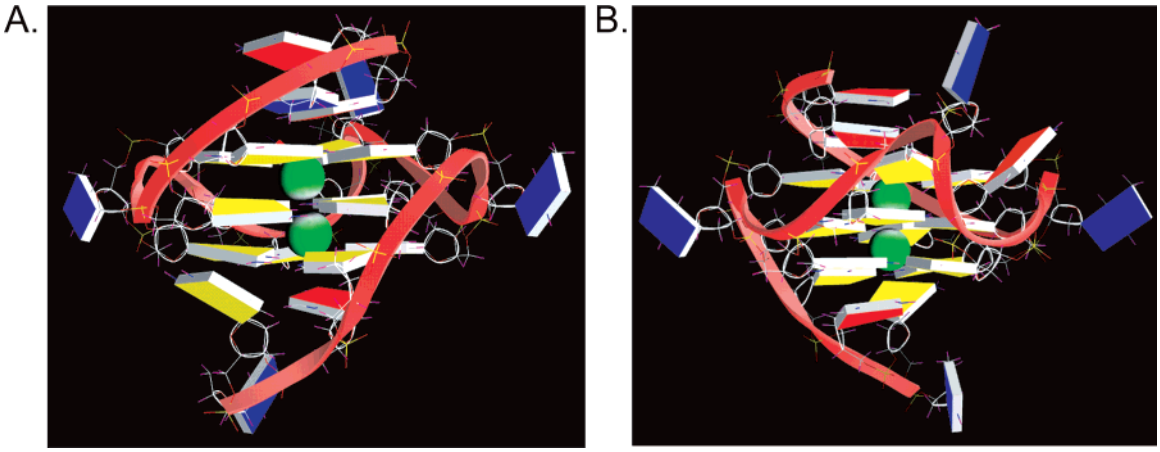

FIGURE 8: A representative model of the NMR-refined MYC22-G14T/G23T parallel-stranded G-quadruplex structure in two opposite views, prepared using the program GRASP (*31*). Two potassium ions are included for the calculation (green spheres between the G-tetrads). (A) Viewing from the tetrad groove with no loop. The two flanking sequences capping each end of the G-quadruplex are clearly seen. (B) Viewing from the tetrad groove where the double nucleotide TA loop is located. The two single T side loops and the double nucleotide TA loop are clearly seen. Guanine = yellow, adenine = red, thymine = blue.

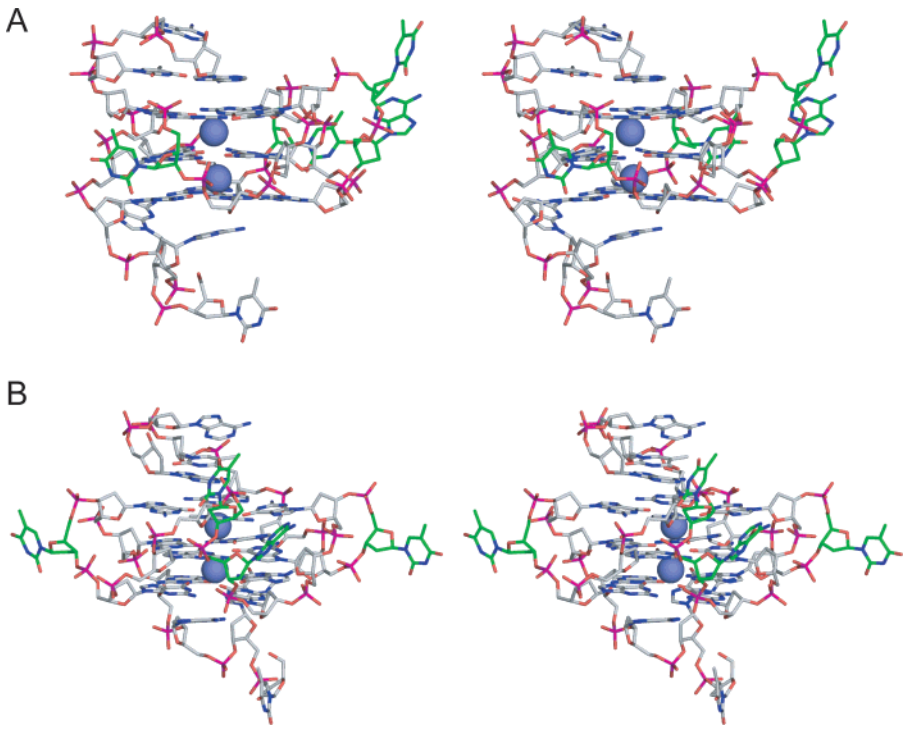

FIGURE 9: Two stereoviews showing the double-chain reversal loop structures of the MYC22-G14T/G23T parallel-stranded G-quadruplex. Two potassium ions are included for the calculation (green spheres between the G-tetrads). (A) Viewing from the first single-T double-chain reversal loop. (B) Viewing from the double nucleotide TA double-chain reversal loop. Nitrogen atoms are blue, oxygen atoms are red, and phosphorus atoms are magenta. Carbon atoms of loop regions are green, and the rest carbon atoms are gray.

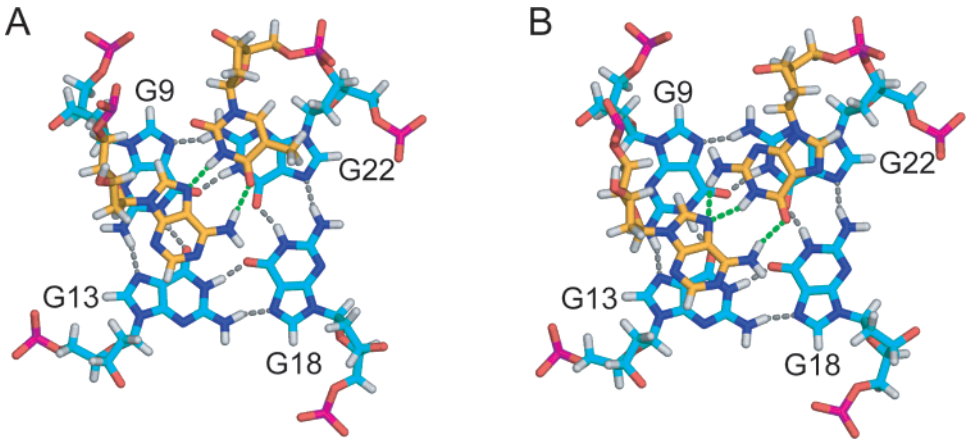

FIGURE 10: The top view of the G-quadruplex with mutant T23 and wild-type G23. (A) In the MYC22-G14T/G23T double mutant sequence, stacking interactions between the T23:A25 base pair and the top G-tetrad. (B) In the MYC22-G14T sequence, stacking interactions between the wild-type G23:A25 base pair and the top tetrad. The guanines of the top tetrad are labeled. The hydrogen bonds of the top-tetrad (black) and the T/G23:A25 base pair (green) are represented in dashed lines. Nitrogen atoms are blue, oxygen atoms are red, phosphorus atoms are magenta, and hydrogen atoms are white. Carbon atoms of G-tetrad are cyan and carbon atoms of 3′-flanking sequence are orange.

handed sugar phosphate backbone twist, while the A24 residue is further stacked with the T23:A25 base pair. Interestingly, the T23 base is paired with A25 using Hoogsteen-type hydrogen bonds. Weak imino peaks are observed at 10 °C in H_2O; however, they cannot be well characterized due to broad line widths.

The 5′-TGA flanking sequence adopts a more or less left-handed twist backbone conformation, which is also evident from the NOE connectivities of this overhanging sequence as discussed previously. The A6 residue stacks very well with G7 of the bottom tetrad, while the G5 residue is positioned on the side of G7 and G20. The 3′-terminal T4 is located further toward the solvent.

Biological Relevance of the MYC22-G14T/G23T G-Quadruplex Structure. Both 3′- and 5′-flanking sequences form stable conformations and function as terminal caps of the G-quadruplex, which are important for the extreme stability of this structure. In both D_2O exchange and VT experiments, the imino protons of G20 (bottom tetrad) and G22 (top tetrad) show better stability than those of other guanines from the top and bottom tetrads (Figures 8 and 9). This observation is in accord with our molecular structure, as the G20 and G22 are the two bases protected by the 3′- and 5′-flanking nucleotide caps, namely, the T23:A25 base pair and the A6 residue, respectively (Figure 10A).

The 5′-G5 and A6 residues, which are involved in the capping function, are the same residues in the wild-type

c-MYC silencer element and are therefore biologically relevant. The T23, which is involved in the fold-back structure of the 3′-flanking TAA sequence, is a mutation from the wild-type G23. To test the effect of the wild-type G23, we have carried out energy minimization and molecular dynamics calculations of our G-quadruplex structure by replacing T23 with G23. The 3′-flanking GAA sequence, as occurs in the wild-type Pu27-mer, can also form a similar stable fold-back conformation. G23 is nicely base-paired with A25, where O6 of G23 is H-bonded with amino H61 of A25, and both NH1 and amino H21 of G23 form bidentate H-bonds with N7 of A25 (Figure 10B).

This capping effect explains the mechanism by which the addition of extra nucleotides can enhance the stability of the quadruplex structure. The melting temperature of MYC22-G14T/G23T is over 85 °C, very close to the melting temperature of the wild-type Pu27, whereas the melting temperature of Pu18-G14T/G23T is around 70 °C (*15*) (sequences shown in Figure 1). All these data indicate that our G-quadruplex structure may be biologically relevant, since the wild-type c-MYC promoter DNA, as exemplified by the Pu27-mer, has extended flanking DNA sequences at both ends of the G-rich region and therefore can adopt the needed capping conformations to stabilize the major G-quadruplex conformation. As the Pu27 is located in the intact promoter of c-MYC within a duplex region, it is unlikely that the DNA strands change conformation abruptly from G-quadruplex to duplex structure; therefore, it is highly possible that a transition region, such as the capping structure, can be formed at the junction interface.

Implication for Cancer Drug Target and Drug Binding. The NHE III_1 c-MYC silencer element has been shown to be a good cancer drug target, and the quadruplex-interacting agents that stabilize this silencer element can potentially inhibit c-MYC oncogene expression (*12*−*14*). However, a structure-based approach toward development of quadruplex-interacting agents specifically targeting this c-MYC silencer element requires a well-defined drug target and the atomic level information on the structure of the biologically relevant G-quadruplex.

For the purpose of drug design, this particular sequence should be considered as the best molecular system for the G-rich c-MYC silencer element, not only because it represents the predominant conformation of the c-MYC G-quadruplex, but also because this molecule is shown to have excellent NMR properties (narrow line widths, good resolution, clean spectra). Furthermore, the double mutation in this sequence eliminates the possible dynamic mixture of various G-quadruplex structures.

ACKNOWLEDGMENT

We thank Dr. Laurence H. Hurley and his lab for valuable assistance and discussion. We thank Dr. David Bishop and Dr. Megan Carver for proofreading the manuscript.

SUPPORTING INFORMATION AVAILABLE

HMQC experiments for base imino H1 proton assignments, H_2O-D_2O exchange experiments, and multiple conformations shown in NOESY spectra at 10 °C. This material is available free of charge via the Internet at http://pubs.acs.org.

REFERENCES

1. Facchini, L. M., and Penn, L. Z. (1998) The molecular role of Myc in growth and transformation: recent discoveries lead to new insights, *FASEB J. 12*, 633−651.
2. Pelengaris, S., Rudolph, B., and Littlewood, T. (2000) Action of Myc in vivo−proliferation and apoptosis, *Curr. Opin. Genet. Dev. 10*, 100−105.
3. Spencer, C. A., and Groudine, M. (1991) Control of c-myc regulation in normal and neoplastic cells, *Adv. Cancer Res. 56*, 1−48.
4. Marcu, K. B., Bossone, S. A., and Patel, A. J. (1992) Myc function and regulation, *Annu. Rev. Biochem. 61*, 809−858.
5. Cooney, M., Czernuszewicz, G., Postel, E. H., Flint, S. J., and Hogan, M. E. (1988) Site-specific oligonucleotide binding represses transcription of the human c-Myc gene in vitro, *Science 241*, 456−459.
6. Simonsson, T., Pribylova, M., and Vorlickova, M. (2000) A nuclease hypersensitive element in the human c-myc promoter adopts several distinct i-tetraplex structures, *Biochem. Biophys. Res. Commun. 278*, 158−166.
7. Simonsson, T., Pecinka, P., and Kubista, M. (1998) DNA tetraplex formation in the control region of c-myc, *Nucleic Acids Res. 26*, 1167−1172.
8. Tomonaga, T., and Levens, D. (1996) Activating transcription from single stranded DNA, *Proc. Natl. Acad. Sci. U.S.A. 93*, 5830−5835.
9. Michelotti, E. F., Tomonaga, T., Krutzsch, H., and Levens, D. (1995) Cellular nucleic acid binding protein regulates the CT element of the human c- myc protooncogene, *J. Biol. Chem. 270*, 9494−9499.
10. Postel, E. H., Berberich, S. J., Rooney, J. W., and Kaetzel, D. M. (2000) Human NM23/nucleoside diphosphate kinase regulates gene expression through DNA binding to nuclease-hypersensitive transcriptional elements, *J. Bioenerg. Biomembr. 32*, 277−84.
11. Collins, I., Weber, A., and Levens, D. (2001) Transcriptional consequences of topoisomerase inhibition, *Mol. Cell. Biol. 21*, 8437−8451.
12. Siddiqui-Jain, A., Grand, C. L., Bearss, D. J., and Hurley, L. H. (2002) Direct evidence for a G-quadruplex in a promoter region and its targeting with a small molecule to repress c-MYC transcription, *Proc. Natl. Acad. Sci. U.S.A. 99*, 11593−11598.
13. Grand, C. L., Han, H., Munoz, R. M., Weitman, S., Von Hoff, D. D., Hurley, L. H., and Bearss, D. J. (2002) The cationic porphyrin TMPyP4 down-regulates c-MYC and human telomerase reverse transcriptase expression and inhibits tumor growth in vivo, *Mol. Cancer Ther. 1*, 565−573.
14. Grand, C. L., Powell, T. J., Nagle, R. B., Bearss, D. J., Tye, D., Gleason-Guzman, M., and Hurley, L. H. (2004) Mutations in the G-quadruplex silencer element and their relationship to c-MYC overexpression, NM23 repression, and therapeutic rescue, *Proc. Natl. Acad. Sci. U.S.A. 101*, 6140−6145.
15. Seenisamy, J., Rezler, E. M., Powell, T. J., Tye, D., Gokhale, V., Joshi, C. S., Siddiqui-Jain, A., and Hurley, L. H. (2004) The dynamic character of the G-quadruplex element in the c-MYC promoter and modification by TMPyP4, *J. Am. Chem. Soc. 126*, 8702−8709.
16. Phan, A. T., Modi, Y. S., and Patel, D. J. (2004) Propeller-type parallel-stranded G-quadruplexes in the human c-myc promoter, *J. Am. Chem. Soc. 126*, 8710−8716.
17. Zhao, H., Pagano, A. R., Wang, W. M., Shallop, A., Gaffney, B. L., and Jones, R. A. (1997) Use of a ^{13}C atom to differentiate two ^{15}N-labeled nucleosides. Syntheses of [$^{15}NH_2$]-adenosine, [1,-NH_2-$^{15}N_2$]- and [2-^{13}C-1,NH_2-$^{15}N_2$]-guanosine, and [1,7,NH_2-$^{15}N_3$]- and [2-^{13}C-1,7,NH_2-$^{15}N_3$]-2′-deoxyguanosine, *J. Org. Chem. 62*, 7832−7835.
18. Maple, J. R., Hwang, M. J., Jalkanen, K. J., Stockfisch, T. P., and Hagler, A. T. (1998) Derivation of class II force fields: V. Quantum force field for amides, peptides, and related compounds, *J. Comput. Chem. 19*, 430−458.
19. Smith, F. W., and Feigon, J. (1992) Quadruplex structure of *Oxytricha* telomeric DNA oligonucleotides, *Nature 356*, 164−168.
20. Matsugami, A., Ouhashi, K., Kanagawa, M., Liu, H., Kanagawa, S., Uesugi, S., and Katahira, M. (2001) An intramolecular

quadruplex of $(GGA)_4$ triplet repeat DNA with a G:G:G:G tetrad and a G(:A)G(:A):G(:A):G heptad, and its dimeric interaction, *J. Mol. Biol. 313*, 255−269.
21. Scaria, P. V., Shire, S. J., and Shafer, R. H. (1992) Quadruplex structure of $d(G_3T_4G_3)$ stabilized by K^+ or Na^+ is an asymmetrichairpin dimer, *Proc. Natl. Acad. Sci. U.S.A. 89*, 10336−10340.
22. Marathias, V. M., and Bolton, P. H. (2000) Structures of the potassium-saturated, 2:1, and intermediate, 1:1, forms of a quadruplex DNA, *Nucleic Acids Res. 28*, 1969−1977.
23. Gavathiotis, E., Heald, R. A., Stevens, M. F. G., and Searle, M. S. (2003) Drug recognition and stabilisation of the parallel-stranded DNA quadruplex $d(TTAGGGT)_4$ containing the human telomeric repeat, *J. Mol. Biol. 334*, 25−36.
24. Wang, Y., and Patel, D. J. (1993) Solution structure of the human telomeric repeat $d[AG_3(T_2AG_3)_3]$ G-tetraplex, *Structure 1*, 263−282.
25. Parkinson, G. N., Lee, M. P. H., and Neidle, S. (2002) Crystal structure of parallel quadruplexes from human telomeric DNA, *Nature 417*, 876−880.
26. Matsugami, A., Okuizumi, T., Uesugi, S., and Katahira, M. (2003) Intramolecular higher order packing of parallel quadruplexes comprising a G:G:G:G tetrad and a G(:A):G(:A):G(:A):G heptad of GGA triplet repeat DNA, *J. Biol. Chem. 278*, 28147−28153.
27. Wang, Y., and Patel, D. J. (1993) Solution structure of a parallel-stranded G-quadruplex DNA, *J. Mol. Biol. 234*, 1171−1183.
28. Macaya, R. F., Schultze, P., Smith, F. W., Roe, J. A., and Feigon, J. (1993) Thrombin-binding DNA aptamer forms a unimolecular quadruplex structure in solution, *Proc. Natl. Acad. Sci. U.S.A. 90*, 3745−3749.
29. Schultze, P., Smith, F. W., and Feigon, J. (1994) Refined solution structure of the dimeric quadruplex formed from the *Oxytricha* telomeric oligonucleotide d(GGGGTTTTGGGG), *Structure 2*, 221−233.
30. Aboulela, F., Murchie, A. I. H., Norman, D. G., and Lilley, D. M. J. (1994) Solution structure of a parallel-stranded tetraplex formed by $d(TG_4T)$ in the presence of sodium-ions by nuclear-magnetic-resonance spectroscopy, *J. Mol. Biol. 243*, 458−471.
31. Nicholls, A., Sharp, K. A., and Honig, B. (1991) Protein folding and association: insights from the interfacial and thermodynamic properties of hydrocarbons, *Proteins: Struct., Funct., Genet. 11*, 281−296.

BI048242P